Clays and Clay Minerals, Vol. 53, No. 3, 278–286, 2005.

URANYL SURFACE COMPLEXES IN A MIXED-CHARGE MONTMORILLONITE: MONTE CARLO COMPUTER SIMULATION AND POLARIZED XAFS RESULTS

JEFFERY A. GREATHOUSE[1,*], HANNAH R. STELLALEVINSOHN[1], MELISSA A. DENECKE[2], ANDREAS BAUER[2] AND ROBERTO T. PABALAN[3]

[1] Department of Chemistry, St. Lawrence University, Canton, NY 13617, USA
[2] Forschungszentrum Karlsruhe GmbH, Institut für Nukleare Entsorgung, Postfach 3640, 76021 Karlsruhe, Germany
[3] Center for Nuclear Waste Regulatory Analyses, Southwest Research Institute, 6220 Culebra Road, San Antonio, TX 78238, USA

Abstract—We report a combined experimental and theoretical study of uranyl complexes that form on the interlayer siloxane surfaces of montmorillonite. We also consider the effect of isomorphic substitution on surface complexation since our montmorillonite sample contains charge sites in both the octahedral and tetrahedral sheets. Results are given for the two-layer hydrate with a layer spacing of 14.58 Å. Polarized-dependent X-ray absorption fine structure spectra are nearly invariant with the incident angle, indicating that the uranyl ions are oriented neither perpendicular nor parallel to the basal plane of montmorillonite. The equilibrated geometry from Monte Carlo simulations suggests that uranyl ions form outer-sphere surface complexes with the $[O=U=O]^{2+}$ axis tilted at an angle of ~45° to the surface normal.

Key Words—Computer Simulation, Monte Carlo, Montmorillonite, Uranyl, X-ray Diffraction, X-ray Absorption Fine Structure.

INTRODUCTION

Safety assessments of nuclear waste disposal as well as environmental management of uranium-contaminated soils (*e.g.* weapons processing plants, uranium mill tailings, *etc.*) require detailed knowledge of retention mechanisms in soils and the subsurface geosphere. Clay minerals are known to be highly efficient at radionuclide retention in natural systems. Their use as backfill material in nuclear waste repositories has also been proposed (Grauer, 1994; Lajudie *et al.*, 1994; Neall *et al.*, 1995). Prediction of U retention on or in clay minerals, *e.g.* smectites, is an essential aspect in safety assessment studies. For reliable predictions of U retention on clay minerals, a thorough understanding of U binding states on or in the clay structure is required. In this study we combine experimental structural characterization of a smectite clay, which was treated with uranyl solutions, using X-ray diffraction (XRD) and polarized X-ray absorption fine structure spectroscopy (P-XAFS) with predictions of structures from Monte Carlo (MC) simulations for uranyl located in a charged montmorillonite interlayer. The P-XAFS results provide metric parameters describing the coordination sphere surrounding uranium. From the polarization dependency of the spectra, the orientation of linear uranyl units ($[O=U=O]^{2+}$) relative to the polarization vector of the incident radiation (ε) can be deduced (Hudson *et al.*, 1996). This information makes it possible to determine if uranyl cations are oriented in a preferred direction to the clay basal plane interlayers (Denecke *et al.*, 2003).

Our simulation methods are based on a previous uranyl-smectite study in which all species were treated as rigid bodies (Zaidan *et al.*, 2003). The MC simulations were used to generate equilibrated interlayer configurations while constant-volume molecular dynamics simulations were used to study the time evolution of uranyl orientation with respect to the clay surface as well as the mobility of $UO_2(H_2O)_5^{2+}$ complexes. The smectite model in that study consisted of charge sites exclusively in the octahedral sheet (*i.e.* Mg for Al substitution). Interlayer uranyl configurations were studied over a range of water content, and the average layer spacing for the two-layer hydrate was in good agreement with XRD values (Tsunashima *et al.*, 1981; Dent *et al.*, 1992). Additionally, $U-O_{eq}$ (equatorial) distances in outer-sphere $UO_2(H_2O)_5^{2+}$ complexes agreed with extended X-ray absorption fine structure (EXAFS) results (Giaquinta *et al.*, 1997; Sylwester *et al.*, 2000). Uranyl complexes underwent several jump-diffusion events over the siloxane surfaces which were accompanied by water exchange within the equatorial shell. The angle between the O=U=O axis and the surface normal were plotted over time and found to fluctuate around a value of 30°. The absence of any angles above 60° ruled out the presence of inner-sphere $UO_2(H_2O)_5^{2+}$ complexes which would have a perpendicular orientation to the surface normal (Zaidan *et al.*, 2003).

The smectite used in the experiments presented here contains a portion of negative charge in the tetrahedral

* E-mail address of corresponding author:
jagreat@sandia.gov
DOI: 10.1346/CCMN.2005.0530307

sheet, unlike the model system studied by Zaidan *et al.* (2003). Additionally, we use density profiles rather than molecular dynamics simulation to determine the average uranyl orientation angle. The rigid body model used in previous simulations (Zaidan *et al.*, 2003) should allow for an accurate comparison with the experimental results, provided that the charge distribution scheme in the clay layers is optimized for tetrahedral substitution. We investigated two charge distribution schemes for a model Na-smectite system before carrying out the uranyl-montmorillonite simulations.

METHODS

Purified homoionic Na-montmorillonite was prepared from Ibeco clay (IKO Minerals GmbH) for use as the starting clay mineral. The Ibeco clay is a smectite with a significant component of tetrahedral charge (35%) and has Ca^{2+} as the dominant exchangeable cation. A detailed description of Ibeco smectite can be found elsewhere (Bauer and Berger, 1998). The clay was first conditioned to remove soluble salts, sparingly soluble minerals and trace cation impurities that potentially could influence the sorption results using the procedure proposed by Baeyens and Bradbury (1997). The purified smectite was then converted into its Na-form (Moore and Reynolds, 1989) and the <2 μm fraction of smectite separated by sedimentation techniques (Day, 1965).

Sorption of uranyl cations on the clay was performed by repeated washing of 0.3 (±0.01) g of the smectite for 24 h with a uranyl nitrate solution (10^{-3} mol/L, $pH_{initial}$ = 3.51), according to the method described by Tsunashima *et al.* (1981). Sorption was observed to be complete after four washings, as indicated by no change >5% in the U concentration of the wash solution before and after treatment. The amount of U loaded onto the clay was determined after extracting the sorbed U from the clay with hot aqua regia. The U concentration in the extracts was measured with an ICP-MS (ELAN 6000). Roughly 0.49 mol U/mol clay were found to be sorbed onto the smectite (45 mg U/g clay).

All chemicals were reagent grade. Uranium (VI) solutions were prepared by dissolution of re-crystallized $UO_2(NO_3)_2 \cdot 6H_2O$. Milli-Q water with a resistivity >18 MΩ cm^{-1} was used throughout. Samples were prepared in air at room temperature and no special measures were taken to exclude carbon dioxide.

XRD

Oriented slides were prepared for XRD by pipetting a slurry of the filtered material onto a glass slide and drying at room temperature overnight. X-ray diffraction scans from 2 to 15°2θ with a step width of 0.02°2θ and 8 s counting time were recorded on a Bruker AXS D8-Advance machine using Cu radiation at 40 kV and 40 mA. Slit sizes were 1°, 0.15° and 1° for aperture slit, receiving slit and scatter slit, respectively.

P-XAFS

Sample preparation followed the method of Dähn *et al.* (2002). To prepare highly oriented films for P-XAFS measurements, 50 mL of the uranyl-clay suspension after four washing treatments were slowly filtered using a 47 mm diameter filter (Millipore, 0.1 μm pore size). Excess salt and aqueous U was removed by careful washing with a few milliliters of Milli-Q water before drying on the filter. To dry the filtered uranyl-sorbed clay, the filter was spanned taut and dried in a desiccator initially over NH_4NO_3 (relative air humidity 63%), followed by two drying cycles over sulfuric acid (first cycle over 5% sulfuric acid at 45°C and the second cycle over 10% sulfuric acid at 30°C). Using this technique, it was possible to create flat disks with a variable but homogeneous thickness and a perfect orientation of the particles. The dried clay was cut into slices and then mounted onto polycarbonate adhesive tape (CMC Klebetechnik GmbH, 23 μm thick), with the slices layered to a stack with a thickness great enough for measurement (eight in all).

Uranium L3 and L1 edge P-XAFS spectra were recorded at room temperature, in transmission mode, at the Hamburger Synchrotronstrahlungslabor, HASYLAB, beamline A1. A Si(311) double-crystal monochromator (DCM) detuned ~50% of the maximum incident flux, was used. The energy was calibrated against the first inflection point in the K edge of a Y foil, defined as 17038.0 eV. The polarization dependency of the XAFS was measured by mounting the samples onto a sample positioner, equipped with a goniometer, enabling positioning of the smectite sample basal planes at varying angles relative to ε. The polarization dependency of the X-ray absorption near edge structure (P-XANES) spectra was recorded at the L3 edge at angles of 0°, 45° and 60° and L1 spectra at 0° and 60°. At the 0° and 45° positions, polarized EXAFS (P-EXAFS) spectra were also recorded at the L3 edge. Due to its small electron transition probability, no P-EXAFS at the L1 edge could be measured for these samples.

The P-XANES and P-EXAFS spectra were extracted from the raw data using standard procedures and the suite of programs EXAFSPAK (George and Pickering, 1995). Theoretical oxygen backscattering amplitude and metal-O phase shift functions, calculated using FEFF7 (Zabinsky *et al.*, 1995), were applied during least-square fits of the P-EXAFS data to the EXAFS equation.

Monte Carlo simulation

Simulations were performed using the code MONTE v3.2 (Skipper, 1996) on an Origin 300 supercomputer (Silicon Graphics, Inc.). Details of our simulation methodology are given previously (Zaidan *et al.*, 2003) and will only be summarized here. Potential parameters for clay, water and uranyl ions are given in our previous study (Zaidan *et al.*, 2003), and those for Na^+ ions are given by Young and Smith (2000). Simulation supercells

https://doi.org/10.1346/CCMN.2005.0530307 Published online by Cambridge University Press

were obtained by randomly adding cations and water molecules to the interlayer region of a $4 \times 2 \times 1$ superlattice of the clay mineral. The dimensions of the supercell were 21.12×18.28 Å in the *ab* plane. Charge-balancing cations (Na^+ or UO_2^{2+}) were initially placed at the midplane. The vertical axis *c* changed while *a* and *b* remain fixed as the system equilibrated to mimic registration of clay layers in an experimental system (Chang *et al.*, 1995). The d_{001} or layer spacing is defined as the average c_z value during the equilibrated portion of the simulation. The system approached an equilibrium configuration through consecutive stages of 50,000 to 500,000 MC steps. Equilibrium data were collected for at least 500,000 additional steps.

RESULTS

XRD

The XRD spectrum for the uranyl-treated Ibeco montmorillonite is shown in Figure 1. The peak position at ~6º corresponds to a *d* spacing of 14.58 Å, in perfect agreement with the mean basal spacing found by Tsunashima *et al.* (1981) for uranyl sorbed between smectite basal planes. Heating to 400ºC for 12 h resulted in loss of all interlayer water with a peak position at ~10 Å. The resulting diffraction pattern was similar to that of illite.

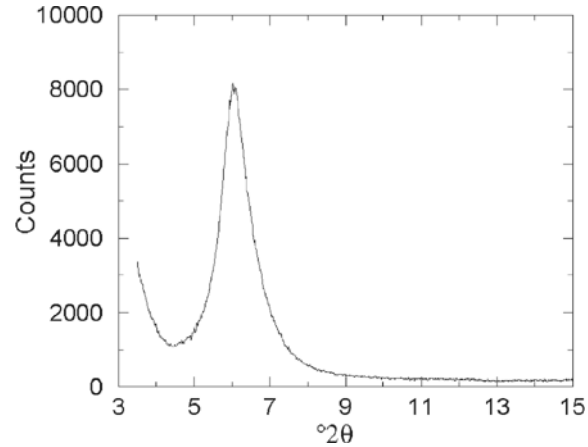

Figure 1. XRD pattern of the uranyl-exchanged smectite. A basal *d* spacing of 14.58 Å was found for the fully exchanged smectites.

P-XAFS

The U L3 and L1 edge P-XANES spectra measured at the angles indicated are shown in Figure 2. The L3 edge

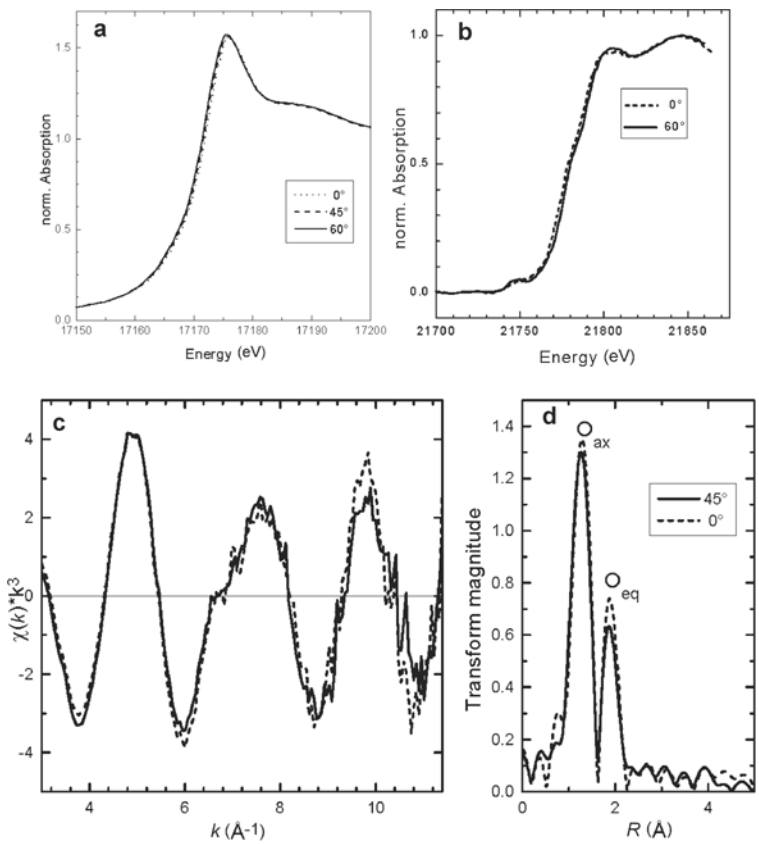

Figure 2. (a) U L3 XANES spectra for a uranyl-exchanged smectite recorded at angles between the clay basal planes and polarization vector indicated. (b) U L1 XANES of the same sample at 0 and 60º. (c) L3 edge k^3-weighted EXAFS oscillations recorded at 0 and 45º and (d) their corresponding Fourier transforms.

https://doi.org/10.1346/CCMN.2005.0530307 Published online by Cambridge University Press

P-XANES show no substantial change with the angle of orientation. No significant change in the intensities of the major absorption feature, the so-called white line (WL) or in the next resonant feature near 17190 eV is observed. In addition, there is only a slight shift in edge energy position with angle. Because of the greater directionality in space of the *p*-like final states for the photoelectron transition at the L1 edge compared to the *d*-like states at the L3 edge, the XANES at the L1 edge is especially sensitive to polarization effects. However, the L1 edge P-XANES of the uranyl exchanged smectite resembles those for non-oriented samples. The L1 P-XANES features in Figure 2 are intermediate between those observed for spectra recorded for samples with uranyl units parallel and those with uranyl units perpendicular to ε (Hudson *et al.*, 1996). The P-XANES spectra exhibit a shoulder on the rising edge and a feature ~20 eV above this. The shoulder corresponds to a sharp peak observed for oriented samples with $[O=U=O]^{2+}$ parallel to ε and the second feature is dominant for an orientation perpendicular to ε. Because both features are evident in Figure 2, we conclude that the average orientation of uranyl units to the smectite basal plane must lie between 0° and 90°.

The P-EXAFS spectra recorded at two orientations of the clay basal plane to ε are also depicted in Figure 2. No Fourier transform (FT) peak for a U−Si interaction is evident, which might be expected for an inner-sphere complex (cf. the 3.6 Å U-Si distance from MC simulations of the inner-sphere complex shown below). The intensity of the FT peak for O atoms in the uranyl cation equatorial plane (O_{eq}) located just below 2 Å (uncorrected for phase shift) is ~14% larger for the spectrum recorded at 0° than that recorded at 45°. The dependency of the P-EXAFS signal amplitude on the angle between ε and the bond axes (Θ) is given by the relationship between the actual coordination number, N, and an effective coordination number, N_{eff}

$$N_{eff} = \tfrac{1}{2}N(1 + 3\cos^2\Theta) \quad (1)$$

$\Theta(U=O_{ax})$ and $\Theta(U-O_{eq})$ define the angle between ε and bond axis of linear uranyl $[O=U=O]^{2+}$ units and between ε and the equatorial plane of the uranyl coordination polyhedron, respectively, and are at right angles to one another. The observed increase in O_{eq} FT amplitude, which we can, according to equation 1, associate with an increase in N_{eff}, could indicate that $\Theta(U-O_{eq})$ at the 0° orientation is smaller than at the 45° orientation. In other words, the equatorial plane is more parallel to ε for the measurement at 0° than it is at 45°. However, there is no corresponding expected decrease in the FT peak for axial O atoms (O_{ax}) going from 0 to 45°, as would be expected from the 90° relation between $\Theta(U=O_{ax})$ and $\Theta(U-O_{eq})$. We conclude that the amplitude change is insignificant and lies within the error margin. Due to uncertainties in background removal, spline-fitting of atomic EXAFS functions, and unknown contributions of multi-electron processes, the largest error associated with the EXAFS method, especially for a single measurement, is in determinations involving amplitude and generally assumed to be of the order of 20−25%.

The lack of significant polarization dependency in the L3 and L1 P-XANES and in the P-EXAFS indicates that sorbed uranyl units are neither perpendicular nor parallel to the smectite clay basal planes. Rather, the $[O=U=O]^{2+}$ molecular axis must be tilted at an angle relative to the basal plane, an effect equated with a tilt near a 'magic' angle. Uranyl units tilted at an angle relative to the basal plane are oriented in all directions over a macroscopic sample volume probed during the measurements. The average structure of the uranium coordination polyhedron 'seen' by ε can be visualized by precession about the axis normal to basal planes with simultaneous rotation about the $[O=U=O]^{2+}$ molecular axis. The averaged structure of the linear $[O=U=O]^{2+}$ unit takes on the form of a double cone and the averaged structure of equidistant O_{eq} atoms takes on the form of a band centered around the node of this double cone. At 0°, 45° and 60°, tilted $[O=U=O]^{2+}$ units' relative alignment to ε does not vary and no spectral changes with angle are observed.

Monte Carlo Simulation

1. Validation of modified clay parameters with Na-vermiculite. In previous simulations of uranyl-smectite complexes, the montmorillonite model consisted of negative charge exclusively in the octahedral sheet (Zaidan *et al.*, 2003). The Ibeco montmorillonite in this study includes negative charge in the tetrahedral sheet as well. Our first task was to investigate the effect of tetrahedral AlO_4 charge parameters on interlayer structure and energy. We chose a simplified vermiculite system based on accurate interlayer structural data on Na-vermiculite, which show that Na^+ ions reside at the midplane (Slade *et al.*, 1985). The simulated system consisted of a single charge site (*i.e.* one tetrahedral AlO_4 unit) one Na^+ ion, and 69 water molecules (two-layer hydrate). The supercell formula for this simplified vermiculite is

$$Na[Si_{63}Al_1](Mg_{48})O_{160}(OH)_{32}\cdot 69H_2O$$

where [ ] refers to the tetrahedral sheet and the first ( ) refers to the octahedral sheet. An initial configuration was obtained by performing a full MC equilibration (Zaidan *et al.*, 2003). For all subsequent Na-vermiculite simulations, the Na^+ ion was placed directly over the tetrahedral Al atom at different z-coordinates. The system was then re-equilibrated, allowing only water molecules to move. The process was repeated for a Na position directly over a coordinating surface O.

We examined two negative charge-distribution schemes, which are described in Table 1. In scheme 1, all negative charge is placed on the Al atom, which is

https://doi.org/10.1346/CCMN.2005.0530307 Published online by Cambridge University Press

Table 1. Atomic charges (in e) for tetrahedral AlO_4 units in MC simulations.

Scheme	Al	O (surface)	O (apical)
1	0.20	−0.80	−1.00
2	1.20	−1.05	−1.25

consistent with previous studies (Skipper *et al.*, 1995; Chang *et al.*, 1995; Karaborni *et al.*, 1996; Greathouse and Sposito, 1998; Greathouse *et al.*, 2000; Chavez-Paez *et al.*, 2001; Hensen and Smit, 2002). In Scheme 2, the negative charge is equally divided among the four neighboring O atoms. The partial charge of each O atom is therefore reduced by 0.25 e. For reference, tetrahedral Si atoms carry a charge of 1.20 e. These two schemes represent the extreme cases of tetrahedral substitution based on the forcefield parameter set of Skipper *et al.* (1995). Average energies with respect to the Na location are shown in Figure 3. For scheme 1, the lowest energy is obtained when the Na^+ ion is near the surface ($z \approx 5.5$ Å) in an inner-sphere surface complex. For scheme 2, the energy is lower when the Na^+ ion is located at or near the midplane ($z \approx 7.3$ Å). This trend is more apparent in Figure 3b when the Na^+ ion is placed above a neighboring O atom. The minimum energies for schemes 1 and 2 are within the standard deviations for these simulations (~8 kcal/mol), so an absolute energy minimum cannot be identified. Energy minima are possible when the Na^+ ion is located at other coordinates on the siloxane surface, but an absolute minimum energy configuration is difficult to identify using the MC algorithm. However, X-ray and neutron diffraction studies (Skipper *et al.*, 1991; Slade *et al.*, 1985) suggest that interlayer Na^+ ions predominate at the midplane, as they do in scheme 2. While this validation method is not capable of ranking the two schemes from an energy standpoint, scheme 2 provides the best agreement with the diffraction studies. Additionally, charge delocalization similar to scheme 2 has recently been used in a flexible clay forcefield (Cygan *et al.*, 2004). Therefore for uranyl-clay simulations we chose scheme 2, in which tetrahedral negative charge is delocalized.

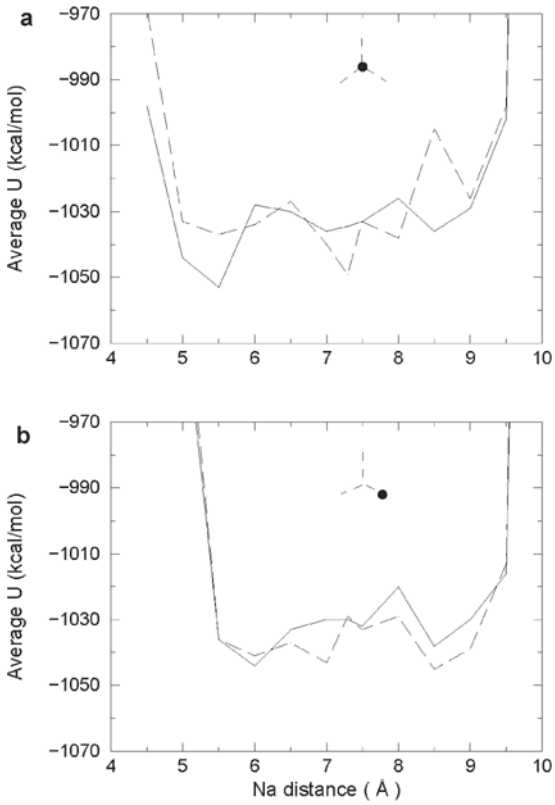

Figure 3. Equilibrium interlayer potential energies from MC simulations with tetrahedral AlO_4 charge for Scheme 1 (solid line) and Scheme 2 (dashed line). The z-coordinate represents the distance from the frozen Na^+ ion to the bottom of the supercell (*i.e.* octahedral cations). Clay surface O atoms are located at $z = 3.28$ Å. The Na^+ ion is positioned directly over the tetrahedral Al atom (a) or directly over a surface O atom (b). The embedded diagrams indicate the location of the Na^+ ion (dark circle) relative to the AlO_4 tetrahedron (dashed line).

2. Simulations of uranyl-Ibeco-montmorillonite. Using scheme 2 for tetrahedral charge sites, we studied a uranyl-montmorillonite system with two tetrahedral charge sites, six octahedral charge sites and four interlayer uranyl ions. The structural and charge properties of the simulated clay correspond to the Ibeco montmorillonite used in the XRD and P-XAFS experiments. Although the fraction of tetrahedral charge (1/4) of the simulated system is slightly less than that of the Ibeco montmorillonite (1/3), we chose to include an even number of such charge sites so that opposing siloxane surfaces are equally charged. Charge sites were randomly located throughout the supercell according to previous studies (Chang *et al.*, 1995; Greathouse and Sposito, 1998). A water content of 63 molecules resulted in an average layer spacing of 14.56±0.05 Å, in agreement with the XRD value of 14.58 Å. The supercell formula is

$$(UO_2)_4[Si_{62}Al_2](Al_{26}Mg_6)O_{160}(OH)_{32}\cdot 63H_2O$$

An equilibrium snapshot is shown in Figure 4a with all uranyl ions centered at the midplane. Each ion forms an outer-sphere complex with five water molecules in the equatorial shell.

Knowing that uranyl-montmorillonite inner-sphere surface complexes are also possible, we performed another simulation in which two uranyl ions were initially placed near the surface. One of the ions was placed near a tetrahedral charge site. A snapshot of this equilibrated system is shown in Figure 4b, showing a monodentate inner-sphere complex at a tetrahedral charge site. Midplane uranyl ions show the familiar coordination shell consisting of five water molecules in the equatorial plane. Unlike the configuration in

https://doi.org/10.1346/CCMN.2005.0530307 Published online by Cambridge University Press

Figure 4a, more water molecules occupy midplane sites. The combination of an inner-sphere complex and midplane water molecules results in a larger d_{001} spacing of 14.70±0.09 Å, which is inconsistent with XRD results.

Averaged radial distribution functions, $g(r)$, for both simulations are shown in Figure 5. The first U−O peak at 2.4 Å consists of five O atoms, as verified by the snapshots (Figure 4). The well-defined exclusion zone from 2.8−3.2 Å, at which $g(r) = 0$, suggests that water molecules do not exchange in the equatorial shell. Molecular trajectories from previous molecular dynamics simulations clearly showed water exchange in the equatorial shell of $[O=U=O]^{2+}$ (Zaidan *et al.*, 2003). Unlike molecular dynamics, however, MC simulations only sample configuration space of equilibrated systems, so we do not expect to see a time-dependent event such as ligand exchange. The equilibrated configuration corresponding to Figure 4b contains an inner-sphere surface complex, so one surface O atom is included in the first U−O peak. However, similarities between the first U−O peaks in Figure 5a,b indicate that the presence of a surface O atom in the

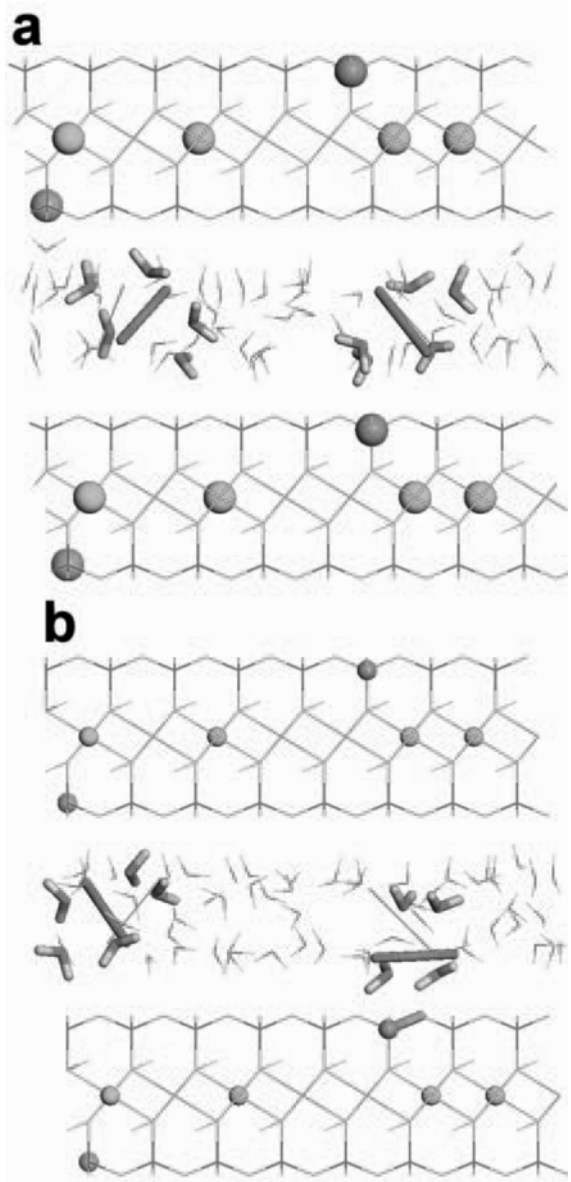

Figure 4. Equilibrium Monte Carlo snapshots of uranyl-Ibeco montmorillonite. The color scheme is as follows; blue − U, pink − Al, red − water O or uranyl O, orange − clay O, green − Si, light blue − Mg, white − H. Negative charge sites are shown as spheres. Two uranyl ions and their equatorial ligands are highlighted. (a) All uranyl ions were initially placed at the midplane. (b) Two uranyl ions were placed near the siloxane surface.

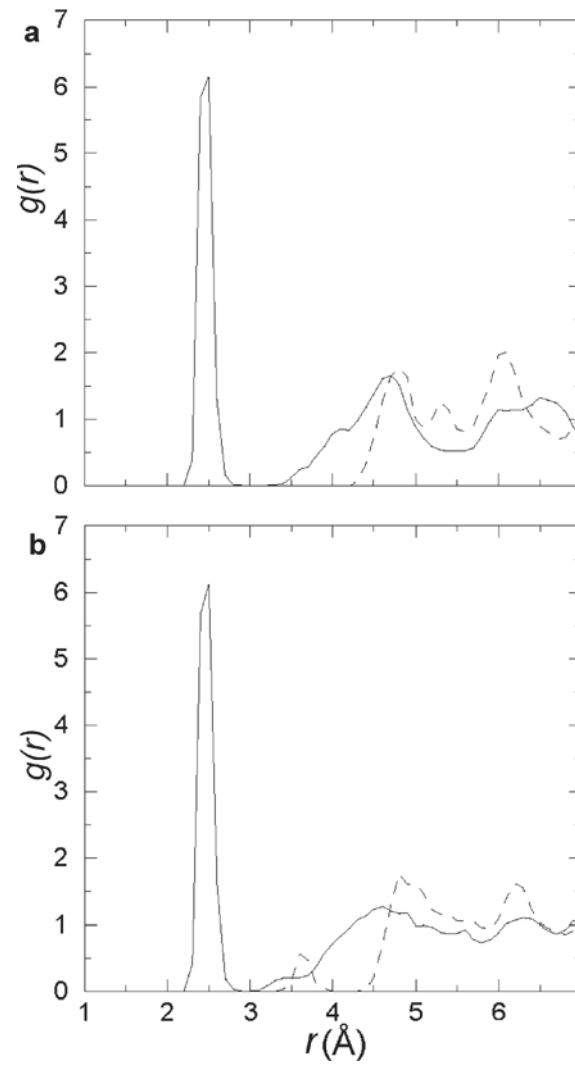

Figure 5. Averaged Monte Carlo radial distribution functions showing U-O (solid line) and U-Si (dashed line) distributions in uranyl-Ibeco montmorillonite. O atoms from both water molecules and the clay layer are included in the U-O distribution. The simulated systems denoted by (a) and (b) correspond to the snapshots shown in Figures 4a and 4b, respectively.

https://doi.org/10.1346/CCMN.2005.0530307 Published online by Cambridge University Press

equatorial shell does not cause a split equatorial shell. We conclude that the U−O (surface) distance is the same as the average U−O (water) distance. The small peak at 3.6 Å in the U−Si distribution (Figure 5b) is due to the single uranyl ion at the surface. The corresponding U−Al distance is 3.3 Å (data not shown). Atomic density profiles in Figure 6 show the probability of finding certain atom types as a function of the height z above the lowermost clay layer (clay surface O atoms are located at z = 3.28 Å and z = 11.28 Å). We show profiles for uranyl atoms only. The uranyl interlayer structure shown in the snapshots (Figure 4) is evident over the entire equilibrated portion of the simulations. Although not shown here, atomic density profiles for water O and H atoms show two well defined water layers, one each above and below the midplane. In Figure 6a, all uranyl ions are centered at the midplane (large peak at 7.15 Å). Their $[O=U=O]^{2+}$ axes are tilted with respect to the surface normal, to facilitate H bonding between equatorial water molecules and both clay surfaces. The average tilt angle (Zaidan *et al.*, 2003) was calculated using uranium and O peak centers and found to be 46±11°. In Figure 6b, the presence of the inner-sphere uranyl surface complex is indicated by the U peak at 5.8 Å. The other three uranyl ions, which reside at the midplane, comprise the large U peak at 7.4 Å. The tilt angle for the inner-sphere uranyl ion is ~90° while that for the three outer-sphere ions is 44±11°.

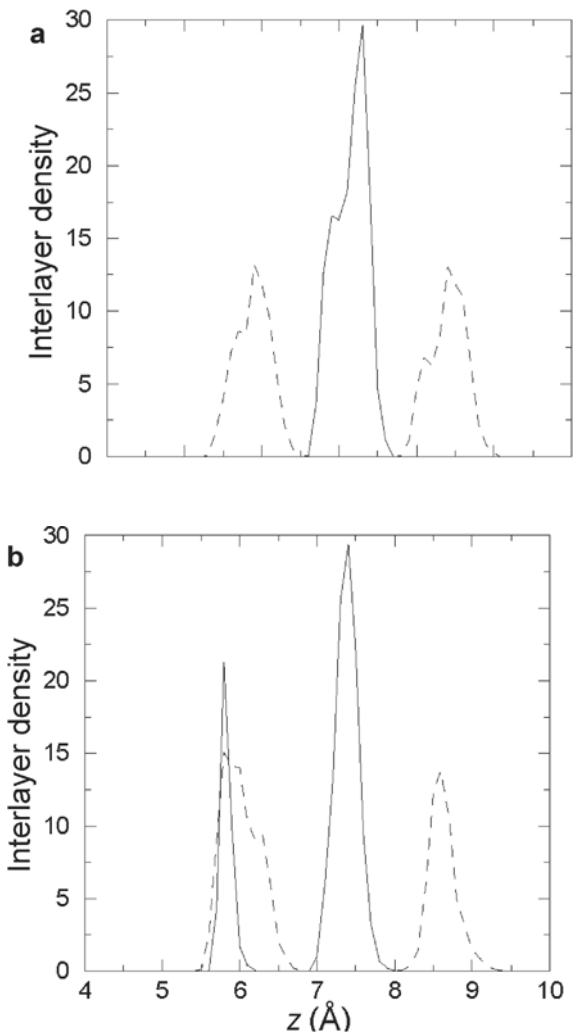

Figure 6. Averaged Monte Carlo atomic density profiles in uranyl-Ibeco montmorillonite. Only uranyl atoms (U, solid line and O, dashed line) are included. The simulated systems denoted by (a) and (b) correspond to the snapshots shown in Figures 4a and 4b, respectively.

CONCLUSIONS

We carried out a comprehensive study of uranyl-smectite surface complexes, combining experimental and simulation results to obtain structural information at the clay-water interface. No clear differentiation between inner-sphere and outer-sphere sorption is possible solely from the lack of U−Si peaks in P-EXAFS. By comparing the layer spacing value from XRD with the simulation results, we are confident that the uranyl ion is interacting with the siloxane surface through an outer-sphere mechanism. If at least one uranyl ion forms an inner-sphere surface complex as in Figure 4b, the simulated layer spacing is larger than the XRD value. The P-XAFS results suggest that the linear uranyl unit is tilted at an angle intermediate between 0 and 90° relative to the surface normal. The simulation results help to identify this average angle to be 45°.

We must explain why uranyl ions prefer to be oriented at an angle of 45° to the clay surface normal as opposed to 0 or 90°. Given the absence of 0 or 90° orientations in the density profiles (Figure 6a), the uranyl rotational barriers from 45 to 90° or from 45 to 0° appear to be quite large. This absence of rotational mobility was confirmed in both the simulation and P-XAFS results. Using MC simulation we cannot identify the energy barrier for the following process near clay surfaces:

$$UO_2(H_2O)_5^{2+}(45°) \rightarrow UO_2(H_2O)_4(O_{clay})^{2+}(90°) + H_2O \quad (2)$$

where O_{clay} refers to a surface O atom. The numbers in parentheses refer to the uranyl tilt angles of 45 and 90° illustrated in Figures 4a and 4b, respectively. Additional static energy calculations or molecular dynamics simulations would help to clarify this issue, as well as the energy barrier for $UO_2(H_2O)_5^{2+}$ rotation about the surface normal. The uranyl complex undergoes large rotational fluctuations with little effect on the system potential energy, but detailed energy minimization calculations would be needed to identify a true lowest energy configuration. However, our MC results, which help to identify the average uranyl orientation, complement the XAFS experiments.

The central issue is the tendency of ions to form inner-sphere or outer-sphere surface complexes. The fact

https://doi.org/10.1346/CCMN.2005.0530307 Published online by Cambridge University Press

that the P-XAFS results rule out the 0 or 90° tilt angles suggests that inner-sphere complexes are not thermodynamically stable. In other words, there is an energy penalty for having a clay basal surface O atom in the equatorial coordination shell of the uranyl ion (equation 2). The MC simulations show that an intermediate tilt angle (45°) is characteristic for outer-sphere complexes. Additional stability for this configuration can be inferred from the tendency of most first-shell water molecules to form H bonds with siloxane surfaces, as seen in Figure 4. Monatomic divalent cations are known to form outer-sphere complexes to maximize water-surface H bonding (Greathouse *et al.*, 2000; Young and Smith, 2000; Greathouse and Storm, 2002), and it appears that the uranyl ion does the same.

ACKNOWLEDGMENTS

This work was supported in part by an award from Research Corporation and in part by the US Nuclear Regulatory Commission (NRC), Office of Nuclear Material Safety and Safeguards, Division of Waste Management, under Contract No. NRC-02-02-012. This paper is an independent product of St. Lawrence University, Forschungszentrum Karlsruhe GmbH and the Center for Nuclear Waste Regulatory Analyses and does not necessarily reflect the views or regulatory position of the NRC. Computational resources were provided in part by the MERCURY supercomputer consortium (http://mars.hamilton.edu) under NSF grant CHE 0116435. We gratefully acknowledge beamtime allotment from HASYLAB and assistance with the experiments from K. Attenkofer, H. Moll and M. Plaschke. We would also like to thank B. Garrison for helpful discussions.

REFERENCES

Baeyens, B. and Bradbury, M.H. (1997) A mechanistic description of Ni and Zn sorption on Na-montmorillonite. 1. Titration and sorption measurements. *Journal of Contaminant Hydrology,* **27**, 199–222.

Bauer, A. and Berger, G. (1998) Kaolinite transformation in high molar KOH solutions. *Applied Geochemistry,* **13**, 905–916.

Chang, F.-R.C., Skipper, N.T. and Sposito, G. (1995) Computer simulation of interlayer molecular structure in sodium montmorillonite hydrates. *Langmuir,* **11**, 2734–2741.

Chavez-Paez, M., Van Workum, K., de Pablo, L. and de Pablo, J.J. (2001) Monte Carlo simulations of Wyoming sodium montmorillonite hydrates. *Journal of Chemical Physics,* **114**, 1405–1413.

Cygan, R.T., Liang, J.-J. and Kalinichev, A.G. (2004) Molecular models of hydroxide, oxyhydroxide, and clay phases and the development of a general force field. *Journal of Physical Chemistry B*, **108**, 1255–1266.

Dähn, R., Scheidegger, A.M., Manceau, A., Curti, E., Baeyens, B., Bradbury, M.H. and Chateigner, D. (2002) Th uptake on montmorillonite: A powder and polarized extended X-ray absorption fine structure (EXAFS) study. *Journal of Colloid and Interface Science*, **249**, 8–21.

Day, P.R. (1965) Particle fractionation and particle size analysis. Pp. 545–567 in: *Methods of Soil Analysis* (C.A. Black, editor). American Society of Agronomy, Inc., Madison, Wisconsin.

Denecke, M.A., Dardenne, K., Lindqvist-Reis, P. and Rothe, J. (2003) Grazing incidence XAFS investigations of Hf(IV) and U(VI) cations sorbed onto mineral surfaces. *Physical Chemistry Chemical Physics,* **5**, 939–946.

Dent, A.J., Ramsay, J.D.F. and Swanton, S.W. (1992) An EXAFS Study of uranyl ion in solution and sorbed onto silica and montmorillonite clay colloids. *Journal of Colloid and Interface Science*, **150**, 45–60.

George, G.N. and Pickering, I.J. (1995) *EXAFSPAK: A Suite of Computer Programs for Analysis of X-ray Absorption Spectra*. Stanford Synchrotron Radiation Laboratory, Stanford, California, USA.

Giaquinta, D.M., Soderholm, L., Yuchs, S.E. and Wasserman, S.R. (1997) The speciation of uranium in a smectite clay: evidence for catalysed uranyl reduction. *Radiochimica Acta*, **76**, 113–121.

Grauer, R. (1994) Bentonite as a backfill material in a high-level waste repository. *MRS Bulletin*, **19**, 43–46.

Greathouse, J.A. and Sposito, G. (1998) Monte Carlo and molecular dynamic simulations of interlayer structure in $Li(H_2O)_3$-smectites. *Journal of Physical Chemistry B*, **102**, 2406–2414.

Greathouse, J.A. and Storm, E.W. (2002) Calcium hydration on montmorillonite clay surfaces studied by Monte Carlo simulation. *Molecular Simulation*, **28**, 633–647.

Greathouse, J.A., Refson, K. and Sposito, G. (2000) Molecular dynamics simulation of water mobility in magnesium-smectite hydrates. *Journal of the American Chemical Society*, **122**, 11459–11464.

Hensen, E.J.M. and Smit, B. (2002) Why clays swell. *Journal of Physical Chemistry B*, **106**, 12664–12667.

Hudson, E.A., Allen, P.G., Terminello, L.J., Denecke, M.A. and Reich, T. (1996) Polarized x-ray absorption spectroscopy of the uranyl ion: comparison of experiment and theory. *Physical Review B*, **54**, 156–165.

Karaborni, S., Smit, B., Heidug, W., Urai, J. and van Oort, E. (1996) The swelling of clays: molecular simulations of the hydration of montmorillonite. *Science*, **271**, 1102–1104.

Lajudie, A., Raynal, J., Petit, J.-C. and Toulhoat, P. (1994) Clay-based materials for engineered barriers: A review. Pp. 221–231 in: *Scientific Basis for Nuclear Waste Management XVIII* (T. Murakami and R.C. Ewing, editors). Materials Research Society, Pittsburgh, Pennsylvania, USA.

Moore, D.M. and Reynolds, R.C., Jr. (1989) *X-ray Diffraction.* Oxford University Press, Oxford and New York, p. 322.

Neall, F.B., Baertschi, P., McKinley, I.G., Smith, P.A., Sumerling, T. and Umeki, H. (1994) Comparison of the concepts and assumptions in five recent HLW/spent fuel performance assessments. Pp. 503–510 in: *Scientific Basis for Nuclear Waste Management XVIII* (T. Murakami and R.C. Ewing, editors). Materials Research Society, Pittsburgh, Pennsylvania, USA.

Skipper, N.T. (1996) *MONTE User's Manual.* Department of Physics and Astronomy, University College London, UK.

Skipper, N.T., Soper, A.K. and McConnell, J.D.C. (1991). The structure of interlayer water in vermiculite. *Journal of Chemical Physics*, **94**, 5751–5760.

Skipper, N.T., Chang, F.-R.C. and Sposito, G. (1995) Monte Carlo simulation of interlayer molecular structure in swelling clay minerals. 1. methodology. *Clays and Clay Minerals*, **43**, 285–293.

Slade, P.G., Stone, P.A. and Radoslovich, E.W. (1985) Interlayer structures of the two-layer hydrates of Na- and Ca-vermiculites. *Clays and Clay Minerals*, **33**, 51–61.

Sylwester, E.R., Hudson, E.A. and Allen, P.G. (2000) The structure of uranium (VI) sorption complexes on silica, alumina, and montmorillonite. *Geochimica et Cosmochimica Acta*, **64**, 2431–2438.

Tsunashima, A., Brindley, G.W. and Bastovanov, M. (1981) Adsorption of uranium from solutions by montmorillonite:

compositions and properties of uranyl montmorillonites. *Clays and Clay Minerals*, **29**, 10–16.

Young, D.A. and Smith, D.E. (2000) Simulations of clay mineral swelling and hydration: dependence upon interlayer ion size and charge. *Journal of Physical Chemistry B*, **104**, 9163–9170.

Zabinsky, S.I., Rehr, J.J., Ankudinov, A., Albers, R.C. and Eller, M.J. (1995) Multiple-scattering calculations of x-ray-absorption spectra. *Physical Review B*, **52**, 2995–3009.

Zaidan, O.F., Greathouse, J.A. and Pabalan, R.T. (2003) Monte Carlo and molecular dynamics simulation of uranyl adsorption on montmorillonite clay. *Clays and Clay Minerals*, **51**, 372–381.

(*Received 9 March 2004; revised 17 January 2005; Ms. 891; A.E. Randall T. Cygan*)